Macromolecules

Article

pubs.acs.org/Macromolecules

Synthesis, Morphology, and Properties of Segmented Poly(ether amide)s with Uniform Oxalamide-Based Hard Segments

Niels J. Sijbrandi,[†] Ad J. Kimenai,[‡] Edwin P. C. Mes,[‡] René Broos,[‡] Georg Bar,[§] Martin Rosenthal,[⊥] Yaroslav Odarchenko,[⊥] Dimitri A. Ivanov,[⊥] Pieter J. Dijkstra,*[,†] and Jan Feijen[†]

[†]Department of Polymer Chemistry and Biomaterials, MIRA Institute for Biomedical Technology and Technical Medicine, Faculty of Science and Technology, University of Twente, P.O. Box 217, 7500 AE Enschede, The Netherlands

[‡]Core R&D, DOW Benelux BV, P.O. Box 48, 4530 AA Terneuzen, The Netherlands

[§]Dow Olefin Verbund GmbH, P.O. Box 1163, D-06258, Schkopau, Germany

[⊥]Institut de Sciences des Matériaux de Mulhouse-IS2M, CNRS LRC 7228, Jean Starcky, 15, F-68057 Mulhouse, France

Supporting Information

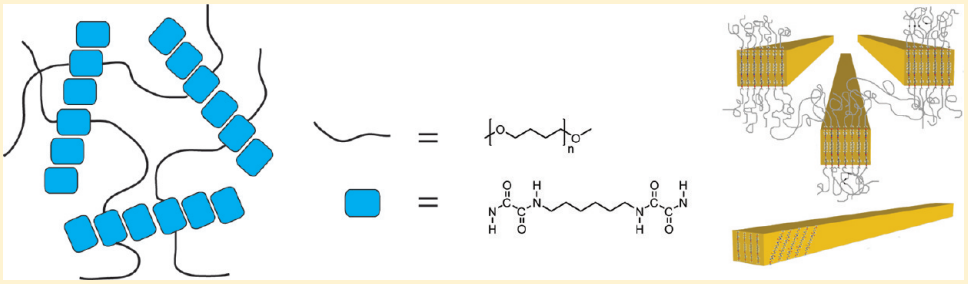

ABSTRACT: The synthesis, morphology, and properties of segmented poly(ether amide)s based on flexible PTHF segments (M_n = 1.1 × 10^3 g mol^{-1}) and uniform rigid oxalamide segments were investigated. The amount of oxalamide groups in the hard segment and the spacer length of bisoxalamide-based hydrogen bonded arrays were varied systematically. The segmented poly(ether amide) with single oxalamide groups connecting the polyether blocks was a sticky solid with a melting temperature of ∼25 °C. Incorporation of uniform hard segments consisting of two interconnected oxalamide units provided highly phase-separated thermoplastic elastomers with a broad temperature-independent rubber plateau. By decreasing the aliphatic spacer length separating two oxalamide units from 10 to 2 methylene groups, the melting transitions increased from 140 to 200 °C. FT-IR evidenced strongly hydrogen bonded and highly ordered bisoxalamide hard segments with degrees of ordering between 66 and 90%. AFM revealed the presence of fiber-like nanocrystals with lengths up to several hundreds of nanometers randomly dispersed in the soft PTHF matrix. The long dimension of the crystals was found parallel to the direction of the hydrogen bonds. One of the other small dimensions of the crystal approximately equals the length of the oxalamide segment, whereas the other one may correspond to the height of a stack containing ca. 10−20 hydrogen-bonded sheets. Upon heating, the crystalline phase melts over a broad temperature range to give a homogeneous melt according to temperature-dependent FT-IR, SAXS, and rheology data. Increasing the number of oxalamide groups in the hard segment to three afforded a highly phase-separated material with a melting transition above 200 °C. The segmented copolymers with two or three oxalamide groups in the hard segment show a distinct yield point and have an elastic modulus between 121 and 210 MPa, a stress at break ranging from 15 to 27 MPa, and strain at break of 150 up to 900%. The results demonstrate that alternating block copolymers with soft PTHF segments and uniform hard segments containing two or three oxalamide groups are TPEs with good thermal and mechanical properties.

INTRODUCTION

Segmented thermoplastic elastomers consisting of alternating hard and soft segments are melt-processable materials with elastomeric properties at service temperature.[1,2] This is due to the phase-separated morphology, which is induced by the thermodynamic incompatibility of the hard and the soft segments.[3] Aliphatic polyether or polyester chains are often used as the soft segments yielding a continuous matrix with a low T_g, which provide the material with its elastomeric character. The hard segments used can be either polymers or short chains mostly containing urethane, ester, or amide groups. These segments form rigid domains in the soft matrix and act as physical cross-links providing the material with dimensional stability. When the material is heated above the vitrification (in the case of amorphous block copolymer) or melting point (in the case of semicrystalline block copolymers)

Received: October 4, 2011
Revised: January 26, 2012
Published: April 25, 2012

of the hard domains, the polymer becomes a viscous liquid and can be melt processed.

Segmented poly(ether amide)s comprising polyamide-6, polyamide-11, or polyamide-12 hard segments and polytetrahydrofuran, poly(propylene oxide), or poly(ethylene oxide) soft segments are typical examples of segmented thermoplastic elastomers.[1,2] Such polymers have a phase-separated morphology depending on the molecular weight of the polyether and polyamide structural units.[4−21] In general, the polyamide segments crystallize in a lamellar type structure. The segmented copolymers show typical elastomeric properties if the polyether matrix is the continuous phase in which the crystalline polyamide domains are dispersed. The moduli of these materials range from 10 to 30 MPa, the yield strain is between 100 and 200%, and strains at break are above 1000%. Furthermore, the materials exhibit good recoverability, low permanent set, and low mechanical hysteresis. On the other hand, at high polyamide ratios, the hard phase becomes more and more interconnected and polymer properties change to those of typical thermoplastics.[18]

The concentration and molecular weight distribution of the hard segments largely determine the polymer properties. Incomplete phase separation takes place when the polydispersity of the hard segments is high. The shorter segments mainly dissolve in the soft polymer matrix, thereby increasing the glass transition temperature of the material and hence reducing the elastomeric properties. Moreover, the rubber plateau of the polymers becomes temperature dependent and melt transitions are broad. By contrast, segmented block copolymers with uniform hard segments often show an almost complete phase-separated morphology, and therefore these materials possess a much broader thermal service window. Furthermore, the ultimate mechanical properties of these materials are considerably improved compared to materials with nonuniform hard segments.[22−32]

Poly(ether amides) based on PTHF soft segments and uniform amide hard segments like the aramid diamide segment (TΦT) and the tetra-amide segment nylon-6,T (T6T6T) have been extensively studied.[25,33−37] These polymers indeed show a highly phase-separated morphology with fiber-like nanocrystals randomly dispersed in the soft polymer matrix. Even at a low concentration of 3 wt % of hard segment, the polymers show a distinct microphase-separated morphology and true elastomeric properties indicating that the hard domains are effective physical cross-linkers. Similar microphase-separated morphologies have been reported for segmented poly(ether urea)s with uniform hard segments.[28,31]

Oxalamides, diamides of oxalic acid, are good hydrogen-bonding molecules.[38−40] Symmetric oxalamides strongly associate by donating and receiving two hydrogen bonds. The oxalamide group as a hydrogen bonding motif has been utilized in various research areas, like crystal engineering,[38−40] protein engineering,[41−43] organic gelators,[44] and materials science.[45] Because of the conformational rigidity of oxalamide groups, nylon-*x*,2 type materials have high melting temperatures, high moduli, and low solubility, properties of interest for TPEs.[46] To our knowledge, only Schulze has described poly(ether amide)s, PEAs, that contain oxalamide-based hard segments.[47] These polymers were prepared by end-functionalizing Jeffamines (amine-terminated polyethers) with diethyl oxalate followed by melt polycondensation using a variety of diamines. The oxalamide hard segments in these copolymers were not uniform and afforded polymers with properties varying from tough elastic to hard and brittle depending on the polymer composition.

In this paper, we describe the synthesis and structure of novel segmented poly(ether amide)s composed of polytetrahydrofuran flexible polyether segments and uniform oxalamide-based hard segments. The number of oxalamide groups and aliphatic spacer length between oxalamide groups in the hard segment were systematically varied. To understand the structure−property relations of these polymers, the thermal, physical, and mechanical properties have been determined and linked to the phase-separated morphology and crystallization of the oxalamide-based hard segments.

EXPERIMENTAL SECTION

The synthesis and characterization of polymers **2**, **4a**−**e**, and **6** and model compound **8** are described in the Supporting Information.

FT-IR. To minimize the potential oxidation of the material, sample preparation consisted of the following steps. The surface of a 32 × 3 mm NaCl disk (Thermo, International Crystal Laboratories) was roughened to prevent interfering fringes. Subsequently, a polymer solution (0.3−0.5 g mL^{-1}) in dichloromethane was drop-casted on the disk, and the solvent was allowed to evaporate. This step was repeated until the amount of polymer was sufficient to obtain a maximum peak height of 0.5−0.7. The IR sample was placed in the holder, and a second (prepared) disk was put on top. The holder was placed in the cell in an inert atmosphere (N_2 purge glovebag or N_2 purged IR sample compartment). The cell was heated to a temperature 20−50 °C above the T_m of the polymer and subsequently cooled to room temperature. Fourier transform infrared spectra were recorded on a Thermo 5700 spectrometer utilizing a DTGS detector at 4 cm^{-1} resolution. The temperature of the prepared polymer film between sodium chloride windows was controlled by an infrared cell from Spectra Tech (model 0019-019). The data were collected between 4000 and 500 cm^{-1} (16 scans were acquired in each measurement). The graphs were prepared using OPUS 6.1 software. All spectra were normalized to the 2860 cm^{-1} signal. The carbonyl region was analyzed quantitatively in terms of free, bonded, and ordered amide structures by curve fitting (Omnic version 7.2) and following the guidelines of Meier et al.[48] The results are plotted as the relative intensity of the bonded amide versus the total amides.

TGA. Thermal gravimetric analysis was carried out with 5−10 mg samples under a nitrogen atmosphere in the 50−700 °C range at a heating rate of 10 °C min^{-1}, using a Perkin-Elmer thermal gravimetric analyzer TGA 7.

DSC. Thermal analysis was carried out using a Perkin-Elmer Pyris 1. Calibration was carried out with pure indium. Samples (5−10 mg) were heated from −50 to 250 °C at a rate of 20 °C min^{-1}, annealed for 5 min, cooled to −50 °C at a rate of 20 °C min^{-1}, and subsequently heated from −50 to 250 °C at a rate of 20 °C min^{-1}. Melting (T_m) and crystallization (T_c) temperatures were obtained from the peak maxima; melt (ΔH_m) and crystallization (ΔH_c) enthalpies were determined from the area under the curve. The data presented are taken from the first cooling scan and second heating scan.

AFM. Atomic force microscopy images were obtained using a MultiMode scanning probe microscope (SPM) (Veeco Metrology Group, Santa Barbara, CA) with a Nano-Scope IV controller running software version 5.12. The TESP probe used was 125 μm in length and had a tip radius of 8 nm and a force constant of 40 N m^{-1}. A moderate tapping ratio of about 0.5 was applied in all measurements. Height and phase images were recorded at various magnifications. Samples were prepared by drop-casting a 1 mg mL^{-1} chloroform solution on a silicon waver. After evaporation, the sample was heated to 20 °C above the T_{flow} for 15 min and slowly cooled to room temperature.

X-ray Diffraction. Wide-angle X-ray diffraction (WAXD) and small-angle X-ray scattering (SAXS) experiments were conducted on the DUBBLE beamline (BM26B) of the European Synchrotron Radiation Facility in Grenoble, France, using X-ray photons of 10 keV.

dx.doi.org/10.1021/ma2022309 | *Macromolecules* 2012, 45, 3948−3961

Scheme 1. Synthesis of PTHF-OXA (2)

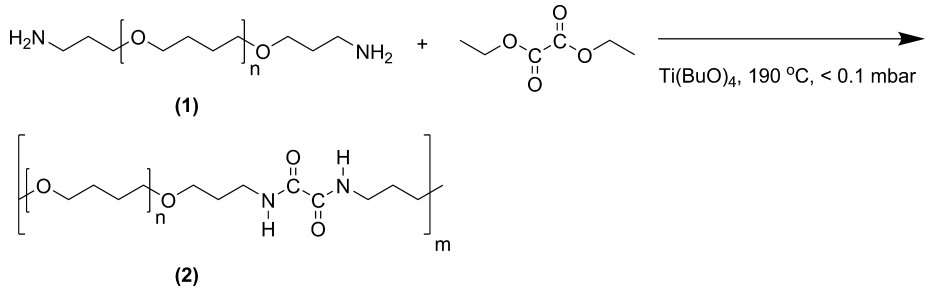

Scheme 2. Synthesis of PTHF-OXA$_2$X with p = 1−5 (4a−e)

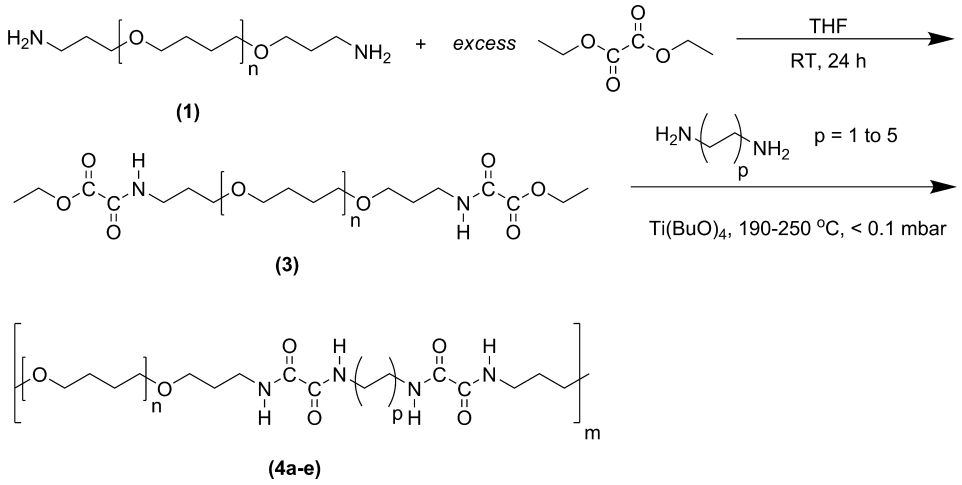

The 2D X-ray patterns were collected in transmission geometry using a 2D multiwire gas-filled detector for the SAXS experiments and a 2D CCD from Photonica for WAXD experiments. For the measurements on the model compound the powder like material was extruded through a die of 300 μm diameter and quickly cooled down to room temperature to prevent reorientation of crystals. The uniaxially oriented material was placed with its fiber axis perpendicular to the incident X-ray beam. The modulus of the scattering vector $\mathbf{s} = 2\sin(\theta/\lambda)$, where θ is the Bragg angle and λ the wavelength, was calibrated using several diffraction orders of silver behenate and corundum for the SAXS and WAXD measurement, respectively. The data reduction and analysis including geometrical and background correction, visualization, and resampling were performed using home-built routines written in Igor Pro software package from WaveMetrics.

Processing. Compression-molded bars (75 × 10 × 2 mm) were prepared using a hot press (THB 008, Fontijne Holland BV, The Netherlands). Polymers were heated for 4 min at ∼20 °C above their T_{flow}, pressed for 3 min at 300 kN, and cooled in ∼5 min under pressure to room temperature.

DMA. Dynamic mechanical analysis was performed using a Myrenne ATM3 torsion pendulum at a frequency of ∼1 Hz. The storage modulus (G') and the loss modulus (G'') were measured as a function of temperature. Samples (50 × 10 × 2 mm) were cooled to −100 °C and then heated at a rate of 1 °C min^{-1}. The temperature at which the loss modulus reached a maximum was taken as the glass transition temperature (T_g). The flow temperature (T_{flow}) was taken at a storage modulus value of 1 MPa.

Tensile Testing. Tensile tests were conducted with compression-molded bars cut to dumbbells (ISO37 type 2). A Zwick Z020 universal tensile machine equipped with a 500 N load cell and extensometers was used to measure the stress at a strain rate of 0.4 s^{-1} (test speed: 60 mm min^{-1}) and a preload of 0.1 MPa. Measurements were performed on at least five different polymer bars.

Rheology. Rheological experiments were performed using an Advanced Rheometric Expansion System (ARES) equipped with parallel plate configuration. Measurements were performed on 25 mm diameter disks punched from 2 mm thick compression-molded plaques. All samples were vacuum-dried for at least 24 h at 60 °C prior to testing. The oven of the ARES was heated to a temperature of ∼20 °C above the melting point of the material. A test specimen was placed between the parallel plates and the top plate was brought into contact with the sample immediately. When the viscosity was very low (normal force dissipates quickly), the sample was trimmed after 1 min. When the normal force was decreasing slowly, a melting time of 3 min was taken before trimming. The total melting time was always 3 min. During melting, the gap between the two plates was adjusted to ∼1.8 mm. All measurements were performed under a nitrogen atmosphere. After an additional 5 min, a frequency sweep was started from 100 to 0.1 rad s^{-1} (logarithmic mode 10 points per decade) with 20% imposed strain. A temperature sweep (cooling trace) was immediately started after the frequency sweep, with a cooling rate of 2 °C min^{-1} to 100 °C, a frequency of 10 rad s^{-1}, and a strain of 20%. The autotension option and autostrain option were both activated to correct the gap and applied strain during solidification of the sample.

RESULTS AND DISCUSSION

Synthesis and Characterization. In the preparation of segmented poly(ether amide)s comprising uniform oxalamide hard segments and polytetrahydrofuran soft segments, three pathways were explored. In the most straightforward approach, diethyl oxalate was polycondensated with an amino end-functionalized polytetrahydrofuran prepolymer (**1**) with a molecular weight (M_n) of 1.1 × 10^3 g mol^{-1} (Scheme 1). In this way, a segmented poly(ether amide) (**2**) was obtained comprising single oxalamide units in the polymer chain.

The polycondensation performed at 190 °C and low pressure resulted in a yellow transparent material in a high yield. In the ^{1}H NMR spectrum of the polymer no signals for the ethyl ester

dx.doi.org/10.1021/ma2022309 | Macromolecules 2012, 45, 3948−3961

Scheme 3. Synthesis of PTHF-OXA$_3$66 (6)

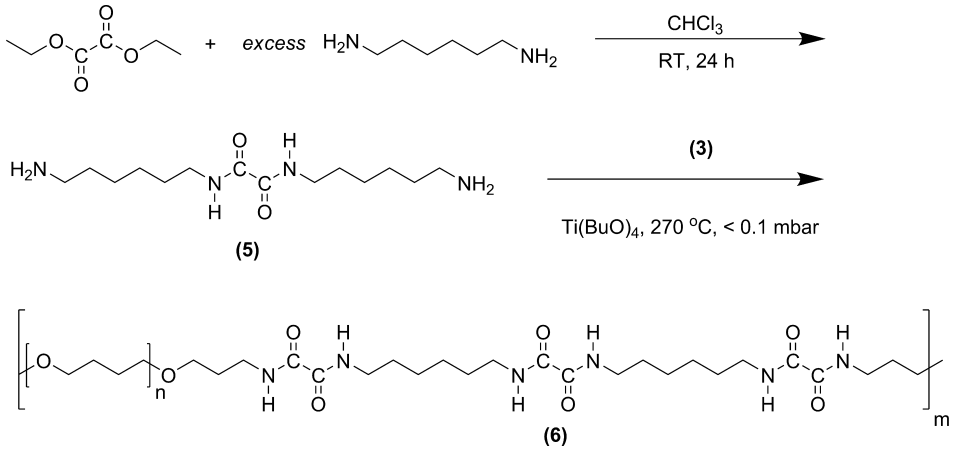

and amino methylene end groups could be observed, indicating that the polymer had a relatively high molecular weight. GPC analysis revealed this material to have a molecular weight of 30 × 10^3 g mol^{-1} with a polydispersity index (PDI) of 9, relative to polystyrene standards.

Despite the relatively high molecular weight polymer that can be obtained, the material was sticky and difficult to handle. To improve the material properties the incorporation of a uniform hard segment with two oxalamide groups in the polymer was investigated. These segmented poly(ether amide)s were prepared in two steps (Scheme 2).

In the first step, an amine end-functionalized polytetrahydrofuran (**1**) was reacted with an excess of diethyl oxalate to convert the amine end groups to the corresponding amide−ester groups (Scheme 2). The use of a 4-fold excess of diethyl oxalate appeared sufficient to avoid polymerization. After removal of the excess of diethyl oxalate by distillation, the material was obtained as a slowly solidifying liquid. The ^{1}H NMR spectrum of the product confirmed full conversion of the amine end groups into the amide−ester end groups by the disappearance of the signal (2.80 ppm) of the methylene protons adjacent to the amino groups. The integral ratio of the amide and ester methylene protons was 1:2, showing that no unwanted polymerization had taken place. ^{13}C NMR spectral data confirmed the structure of the prepolymer. In the carbonyl region, the amide and ester carbonyl carbon atoms are found at δ 157.5 and δ 160.9, respectively. The typical signal of the oxalamide carbonyl carbon atoms as found in **2** (δ 160.1) appeared absent, also demonstrating that polymerization did not take place.

Polycondensation of the newly end-functionalized polytetrahydrofuran (**3**) with aliphatic α,ω-diamines, having 2, 4, 6, 8, and 10 methylene groups, afforded a series of poly(ether amide)s with uniform hard segments comprising two oxalamide groups (**4a**−**e**) (Scheme 2). The polycondensation reactions were performed at 190 °C and low pressure for 4 h for those polymers prepared from diamines with spacer lengths of 6, 8, and 10 methylene groups. To keep the polymerization mixture in the melt, reaction temperatures were increased to 250 and 210 °C for the polymers **4a** and **4b**, respectively. All polymers were obtained as yellow elastic transparent solid materials in high yields. Also in these cases, the absence of peaks for the ethyl ester or amino methylene groups in the ^{1}H NMR spectra of the polymers isolated indicated that the molecular weight of the polymers was relatively high. GPC analysis of the polymers revealed molecular weights in between 23 × 10^3 and 41 × 10^3 g mol^{-1} with PDI's of 9−10 relative to polystyrene standards. The PEAs are very difficult to dissolve in solvents commonly used in GPC due to strong H-bonding interactions. Moreover, the chemical composition of the samples strongly affects their solubility. It turned out that the best solvent is a mixture of 1,1,1,3,3,3-hexafluoro-2-propanol (HFIP) and chloroform. Even in this solvent mixture it is possible that associated structures remain, giving rise to an apparent high molecular weight tail. This might be a reason for the relatively high PDI values found.

In a slightly different way, and based on the easy access to oxalamide end-functionalized PTHF, segmented poly(ether amide)s including three oxalamide groups in the hard segment were prepared (Scheme 3). First a preformed diamine−diamide segment, *N*,*N*′-bis(6-aminohexyl)oxalamide (**5**), was prepared by reacting diethyl oxalate with a 10-fold excess of 1,6-diaminohexane. After purification, the product was obtained as a white powder in a yield of 85%. The polymerization route was similar as described for the preparation of segmented poly(ether amide)s comprising two oxalamide groups in the hard segments. The amide−ester functionalized polytetrahydrofuran **3** was subsequently polycondensated with the diamine−diamide **5**, creating the segmented poly(ether amide) **6** with three oxalamide groups in the hard segment. The polycondensation, when carried out at 270 °C and low pressure for 4 h, provided an elastic transparent solid material in a high yield. The ^{1}H NMR spectra and GPC revealed a molecular weight of 19 × 10^3 g mol^{-1} with a PDI of 10.

FT-IR. In the FT-IR spectra of poly(ether amide)s, the N−H stretching vibration bands at ∼3300 and ∼3400 cm^{-1} can be

Table 1. Molecular Weights of Segmented Poly(ether amide)s 2, 4a−e, and 6

	spacer length	hard segnent content (wt %)	M_n (g mol^{-1} × 10^4)	PDI
PTHF-OXA (**2**)		7.3	3.0	9
PTHF-OXA$_2$6 (**4c**)	6	18.9	4.1	9
PTHF-OXA$_3$66 (**6**)	6 6	27.8	1.9	10
PTHF-OXA$_2$2 (**4a**)	2	15.4	2.3	9
PTHF-OXA$_2$4 (**4b**)	4	17.2	3.0	10
PTHF-OXA$_2$6 (**4c**)	6	18.9	4.1	9
PTHF-OXA$_2$8 (**4d**)	8	20.5	3.2	10
PTHF-OXA$_2$10 (**4e**)	10	22.1	3.2	9

dx.doi.org/10.1021/ma2022309 | *Macromolecules* 2012, 45, 3948−3961

assigned to a hydrogen-bonded and free N−H stretching vibration, respectively (Figure 1).

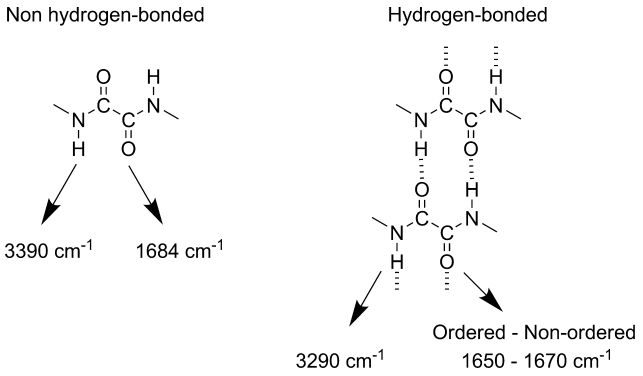

Figure 1. FT-IR wavenumbers of nonbonded and hydrogen-bonded N−H and C═O groups in oxalamides.

These vibrations are not conformationally sensitive, and the broadness of these bands reflects a distribution of hydrogen-bonded groups of varying strength dictated by distance and geometry.[49−51] The poly(ether amide) with single oxalamide units **2** shows a broad hydrogen-bonded N−H band at 3330 cm^{-1} and a shoulder at 3390 cm^{-1} corresponding to free N−H groups. Contrarily, the segmented polymers **4c** and **6** only show a sharp band at 3294 cm^{-1} indicative of the presence of only hydrogen-bonded oxalamide groups (Figure 2).

The amide I band, resulting from C═O stretching vibrations, is also sensitive to the arrangement of H-bonds. Hydrogen-bonded carbonyl groups in the ordered state can be found at 1650 cm^{-1}, whereas disordered hydrogen-bonded and free carbonyl groups shift to higher wavenumbers of 1670 and 1684 cm^{-1}, respectively (Figure 1).

This is illustrated in Figure 2 revealing a broad signal around 1680−1650 cm^{-1} of the poly(ether amide) (**2**) indicative of the presence of free amide species as well as disordered and ordered hydrogen-bonded amide configurations. The ordering of H-bonded amide functionalities in polymers **4c** and **6** is very high as a major sharp signal is found at 1648 cm^{-1}. Thus, FT-IR spectra present evidence for extensive hydrogen bonding and ordering of hard segments consisting of two or three oxalamide groups compared to polymers comprising only single oxalamide units.

In Figure 3, the FT-IR spectra of the segmented poly(ether amide)s with varying spacer lengths between the two oxalamide groups **4a−e** are presented. All five polymers show a sharp N−H stretching band and C═O stretching band at 3296 and 1650 cm^{-1}, respectively, indicating that the major fraction of the oxalamide functional groups reside in a H-bonded and ordered environment. Such observation may be indicative for the presence of at least paracrystalline amide domains, formed by association or stacking of bisoxalamide arrays, and that the degree of phase segregation is high.

The degree of hard segment organization can be estimated by deconvolution of the amide C═O stretching band and calculation of the ratio of the area associated with the hydrogen-bonded ordered amide phase at 1650 cm^{-1} to the total amide absorption area. For the polymers PTHF-$OXA_2$2 (**4a**), PTHF-$OXA_2$4 (**4b**), and PTHF-$OXA_2$10 (**4e**) the molar fraction of ordered hard segments was calculated between 80 and 90% of the total bisoxalamide molar fraction in the polymer, while this value was 66 and 67% for PTHF-$OXA_2$6 (**4c**) and PTHF-$OXA_2$8 (**4d**), respectively. Another characteristic IR band in polyamides is the amide II band, which is a mixed mode with a major contribution of N−H in plane bending and C−N stretching and is found at ∼1530 cm^{-1}. This band is especially sensitive to polymorphism resulting from a significant difference in chain conformation.[52,53] The polymers PTHF-$OXA_2$2 (**4a**) and PTHF-$OXA_2$4 (**4b**) show an amide II band at 1533 cm^{-1}, whereas it is at 1520 cm^{-1} for PTHF-$OXA_2$6, PTHF-$OXA_2$8, and PTHF-$OXA_2$10 (**4c−e**). This suggests that the hard segments with short spacer lengths segregate in a different type of superstructure or develop different paracrystalline order than hard segments with 6, 8, and 10 methylene units between the oxalamide groups. Nylon-*x*,2 polymers are known to crystallize in a fully extended planar zigzag conformation. However, it was shown that chain distortion and hence deviations from the extended conformation increased as the number of methylene groups decreased.[52,53]

With temperature-dependent FT-IR the extent of hydrogen bonding and paracrystalline order of the hard segment was further studied. The N−H stretching vibration band of the polymer PTHF-$OXA_2$6 (**2c**) at different temperatures is depicted in Figure 4a. This polymer had a broad melting transition between 100 and 188 °C in DSC (vide infra, Thermal Properties, DSC). During this transition from 100 °C onward, the N−H stretching band at 3296 cm^{-1} associated with

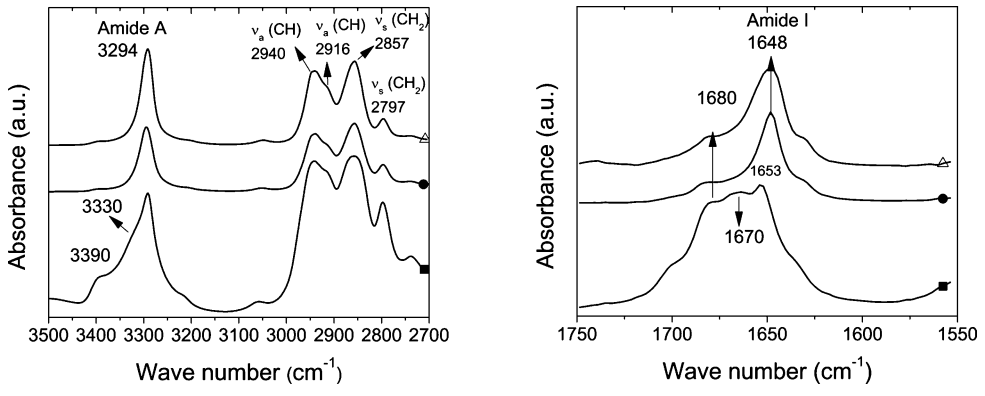

Figure 2. FT-IR spectra of segmented poly(ether amide)s with uniform oxalamide hard segments (■) PTHF-OXA (**2**) at 25 °C, (●) PTHF-$OXA_2$6 (**4c**) at 50 °C, and (△) PTHF-$OXA_3$66 (**6**) at 50 °C.

dx.doi.org/10.1021/ma2022309 | *Macromolecules* 2012, 45, 3948−3961

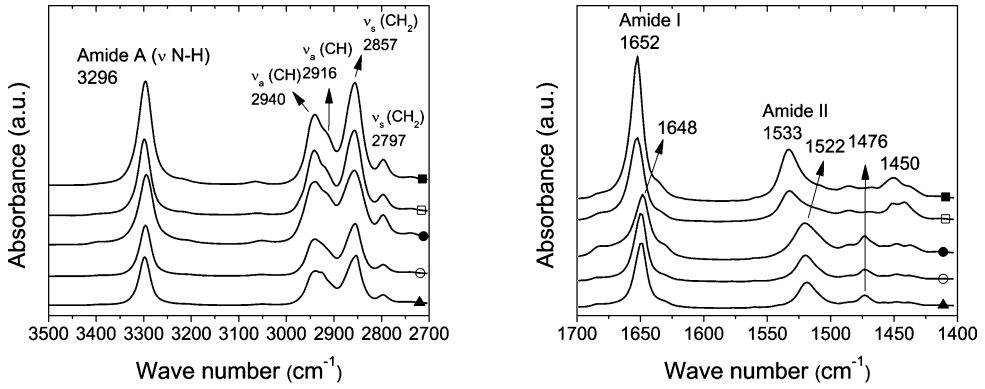

Figure 3. FT-IR spectra at 50 °C of the segmented poly(ether amide)s with two oxalamide groups in the hard segment and with different spacer lengths: (■) PTHF-OXA$_2$2 (**4a**), (□) PTHF-OXA$_2$4 (**4b**), (●) PTHF-OXA$_2$6 (**4c**), (○) PTHF-OXA$_2$8 (**4d**), and (▲) PTHF-OXA$_2$10 (**4e**).

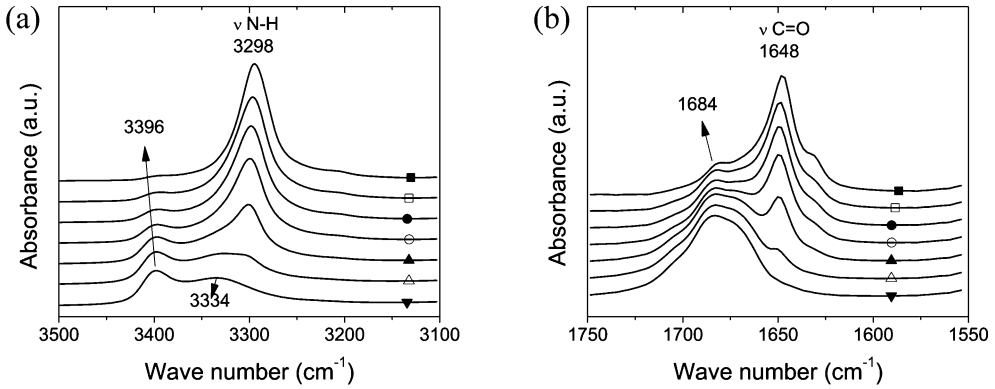

Figure 4. FT-IR spectra of PTHF-OXA$_2$6 (**4c**) at 25 (■), 100 (□), 120 (●), 140 (○), 160 (▲), 180 (△), and 200 °C (▼) for (a) the N−H stretching vibration band and (b) the C═O stretching vibration band.

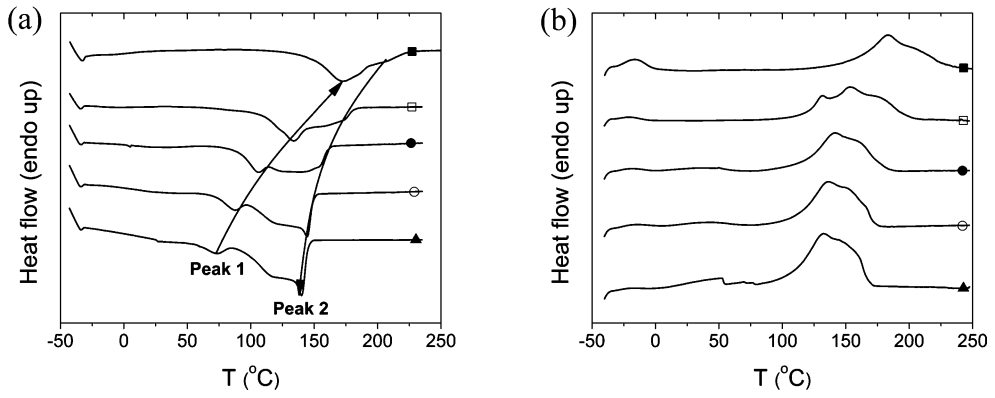

Figure 5. DSC cooling (a) and second heating (b) scans of segmented poly(ether amide)s with two oxalamide groups in the hard segment and with different spacer lengths (■) PTHF-OXA$_2$2 (**4a**), (□) PTHF-OXA$_2$4 (**4b**), (●) PTHF-OXA$_2$6 (**4c**), (○) PTHF-OXA$_2$8 (**4d**), and (▲) PTHF-OXA$_2$10 (**4e**).

amide−amide hydrogen bonding shifts to 3334 cm^{-1} and broadens, indicating that the strength of the hydrogen bonds decreases. In addition, a band at 3396 cm^{-1}, attributed to free N−H groups, arises. At 200 °C, well above the melting transition, still hydrogen bonding appears to be present. The C═O stretching region (Figure 4b) shows similar changes with temperature. Upon increasing the temperature from 100 to 200 °C, the band at 1648 cm^{-1} characteristic for hydrogen-bonded carbonyl groups in the ordered state decreases, whereas the bands associated with hydrogen-bonded disordered carbonyl groups and free carbonyl groups at 1670 and 1684 cm^{-1}, respectively, increase. Such observation seems to agree with the disruption of an crystalline type of order.

Thermal Properties. The thermal stability of the segmented poly(ether amide)s under nonoxidative conditions was determined by thermal gravimetric analysis (TGA). All polymers are stable up to ~410 °C (Table 2). For all polymers the decomposition temperatures are considerably higher than the melting temperatures, which is important for the processing of the materials.

The thermal properties of the segmented poly(ether amide)s were determined by differential scanning calorimetry (DSC). The crystallization and melting temperatures and correspond-

dx.doi.org/10.1021/ma2022309 | *Macromolecules* 2012, 45, 3948−3961

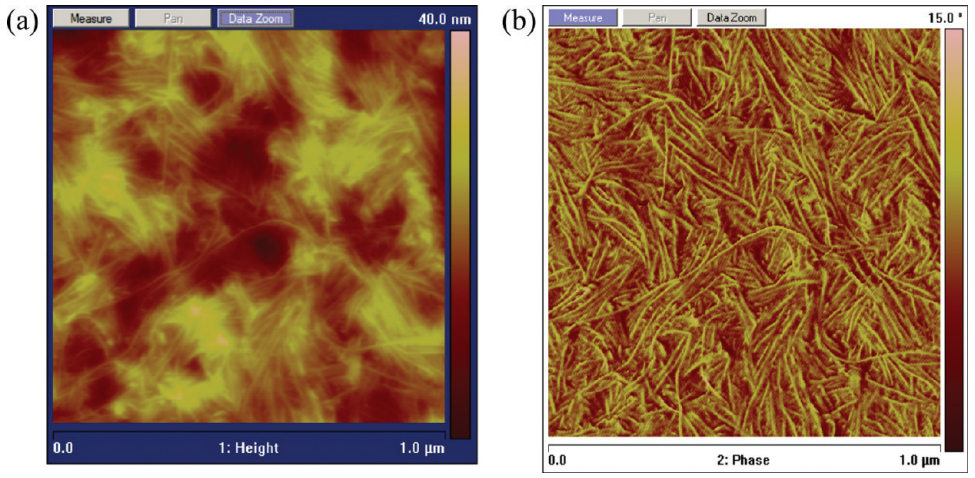

Figure 6. AFM height (a) and phase image (b) of PTHF-$OXA_2$6 (**4c**).

ing enthalpies of the polymers were obtained from the first cooling scan and second heating scan and are reported in Table 2.

Thermal analysis of the segmented copolymers revealed that polymer **2** had a low melting temperature of 18 °C and a crystallization transition at −45 °C. On the other hand, polymer **6** has a high and broad melting transition. Therefore, we have focused our research on the polymers **4a**−**e**. The effect of the spacer length between two oxalamide groups (**4a**−**e**) on the thermal properties of the PEAs is depicted in Figure 5. The T_g values of all copolymers ranged from −65 to −70 °C and were obtained from dynamic mechanical analysis and are listed in Table 4 (vide infra). All polymers have broad melting and crystallization transitions. The presence of multiple transitions suggests that different crystal structures and/or crystal thicknesses are present. Generally, the melting temperature of nylons decreases when the amide-to-methylene ratio decreases, i.e., when the concentration of hydrogen bonds in the polymer chain decreases. This is also observed for the poly(ether amide)s by increasing the length between the oxalamide groups from 2 to 10 methylene units the melting and crystallization temperatures decrease. Upon cooling from the melt, two distinct crystallization transitions were observed (peaks 1 and 2 in Figure 6). With increasing spacer length, both the high and low temperature transitions shift to lower temperatures. Moreover, the lower temperature transition is predominant at shorter spacer lengths, which may be due to the development of a different (para)crystalline superstructure.

Atomic Force Microscopy. The phase image of PTHF-$OXA_2$6 (**4c**) as visualized with atomic force microscopy (AFM) in tapping mode revealed long ribbon-like nanocrystals embedded in the soft polymer matrix (Figure 6). This morphology suggests that crystallization takes place by stacking of the uniform hard segments perpendicular to the fiber axis. Such a morphology is similar to that observed in aramid and nylon-6,T type segmented poly(ether amide)s and segmented poly(ether urea)s with uniform hard segments.[28,31,33,37]

Because the AFM tip has a radius of 8 nm, an accurate determination of the fiber diameter (≤3 nm) was not possible. The length of the crystals is up to several hundreds of nanometers. However, the full length of the crystals cannot be determined since only the surface morphology is visualized.

X-ray Diffraction. We have shown that segmented poly(ether amide)s comprising bisoxalamide or trisoxalamide hard segments are highly phase separated into relatively pure amide and polyether domains. FT-IR measurements revealed that the oxalamide moieties are strongly hydrogen bonded and that the hard segments are highly ordered. Moreover, a fibrillar morphology consisting of ribbon-like nanocrystals randomly dispersed in the polyether matrix was visualized by AFM. These data suggest that the direction along fiber axis is formed by stacking of the hard segments in the direction of the hydrogen bonding.

The phase-separated morphology of the bisoxalamide based poly(ether amide)s (**4a**−**e**) was further investigated by performing wide-angle X-ray diffraction (WAXD) and small-angle X-ray scattering (SAXS) measurements.

To gain more insight into the morphology of the bisoxalamide crystals in the segmented poly(ether amide), a model compound was included in this study consisting of a bisoxalamide array having a spacer length of 6 methylene units and capped with 3-methoxypropyl end groups (MeOProp-$OXA_2$6-PropOMe), **8**. The synthesis of the model compound is displayed in Scheme 4. In the first step, a diester−diamide segment was prepared by reacting 1,6-diaminohexane with a 10-fold excess of diethyl oxalate. Subsequent reaction of the bisoxalamide precursor with 3-methoxypropylamine afforded the model compound **8**. In the model compound the PTHF chains of the polymer are replaced by a methyl group, but the steric and electronic substituent effects on the oxalamide unit are kept the same. Thus, the model compound is thought to show the H-bond-driven organization in the absence of the constraints imposed by the molecular weight of the polymer.

Table 2. Thermal Properties of Segmented Poly(ether amide)s 2, 4a−e, and 6

	T_m (°C)	ΔH_m (J g^{-1})	T_c (°C)	ΔH_m (J g^{-1})	T_{onset} (°C)
PTHF-OXA (**2**)	18		−45		
PTHF-$OXA_2$6 (**4c**)	141/158	34	106/139	34	162
PTHF-$OXA_3$66 (**6**)	189/210	54	134/186	47	225
PTHF-$OXA_2$2 (**4a**)	183/202	36	173/−	30	216
PTHF-$OXA_2$4 (**4b**)	131/174	37	134/−	35	181
PTHF-$OXA_2$6 (**4c**)	141/158	34	106/139	34	162
PTHF-$OXA_2$8 (**4d**)	136/164	35	87/144	34	150
PTHF-$OXA_2$10 (**4e**)	133/−	39	73/140	38	147

dx.doi.org/10.1021/ma2022309 | *Macromolecules* 2012, 45, 3948−3961

Scheme 4. Synthesis of a Bisoxalamide Compound Substituted with 3-Methoxypropyl Moieties

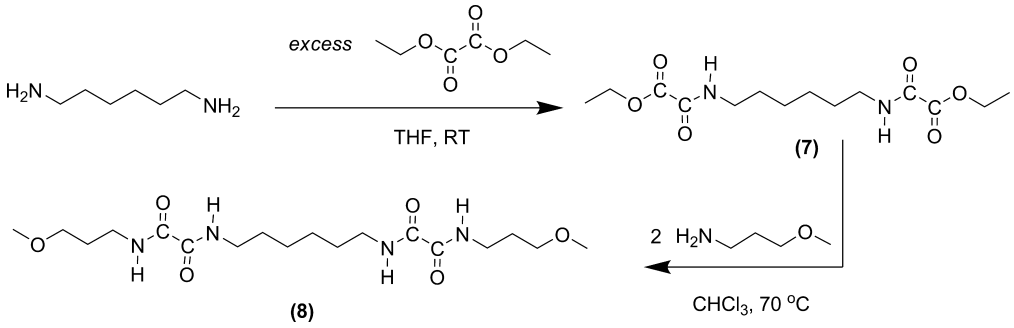

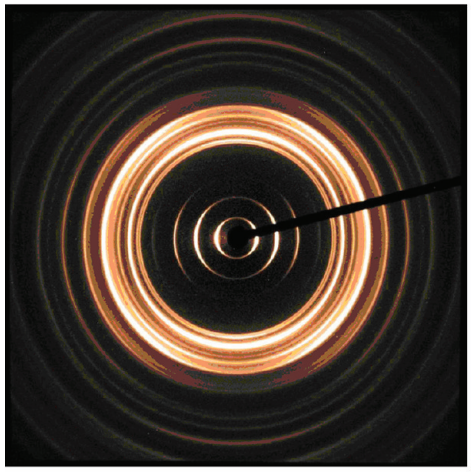

	h	k	l	d_{exp} (Å)	d_{calc} (Å)
equator	0	0	1	22.03	21.98
	0	0	2	10.95	10.99
	0	0	3	7.29	7.33
	0	0	4	5.48	5.49
	0	1	5	4.00	4.02
	0	2	4	3.68	3.70
	0	0	6	3.61	3.66
	0	3	0	3.32	3.33
	0	3	2	3.24	3.19
	0	2	6	2.90	2.96
	0	1	8	2.62	2.65
first	1	0	1	4.79	4.92
layer	1	0	2	4.68	4.59
line	1	1	0	4.36	4.42
	1	1	3	3.83	3.84
	1	1	6	2.85	2.84
	1	3	2	2.73	2.70
second	2	0	0	2.58	2.52
layer	2	0	2	2.49	2.46
line	2	1	2	2.38	2.39
	2	1	3	2.34	2.32
	2	0	4	2.30	2.29
	2	2	2	2.21	2.21

Figure 7. 2D X-ray pattern and its indexation of oriented model compound MeOProp-OXA$_2$6-PropOMe (compound **8**). The fiber axis is vertical.

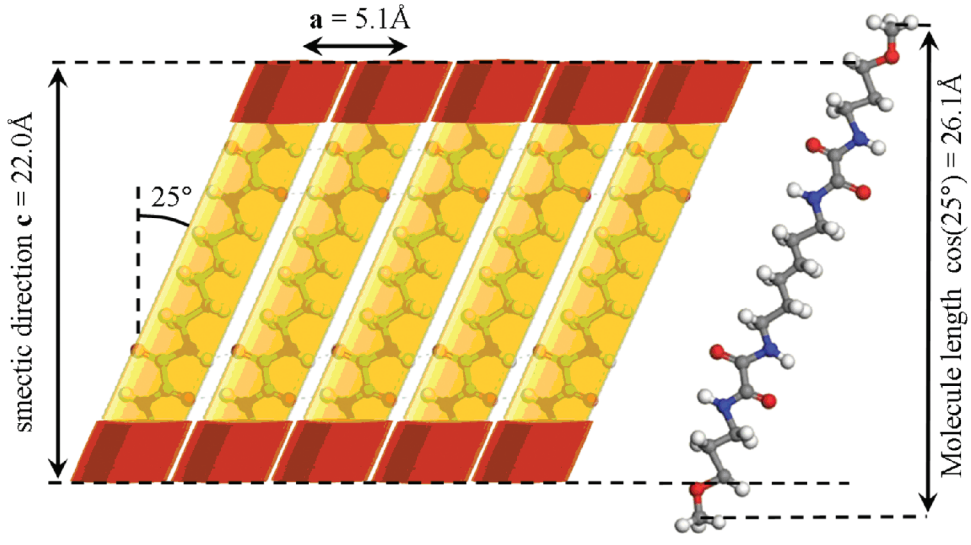

Figure 8. Sketch of the crystalline structure of model compound MeOProp-OXA26-PropOMe (**8**). The fully extended molecular structure is given for the sake of comparison.

dx.doi.org/10.1021/ma2022309 | *Macromolecules* 2012, 45, 3948–3961

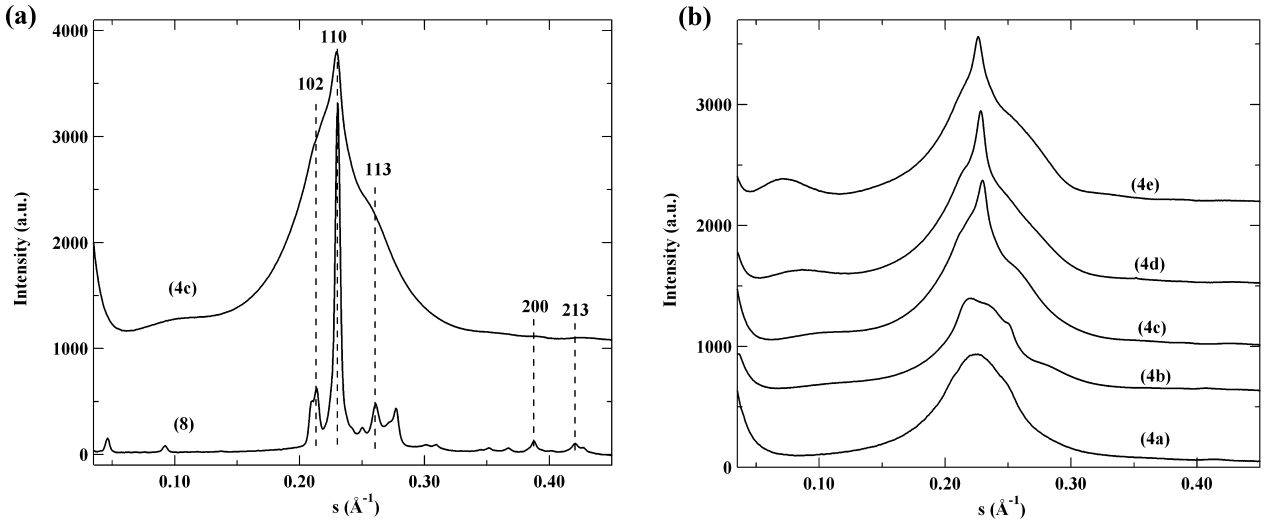

Figure 9. (a) WAXD curves of MeOProp-OXA$_2$6-PropOMe (**8**) and corresponding segmented poly(ether amide) PTHF-OXA$_2$6 (**4c**). (b) WAXD profiles of segmented poly(ether amide)s **4a**−**e** with various hard segment content.

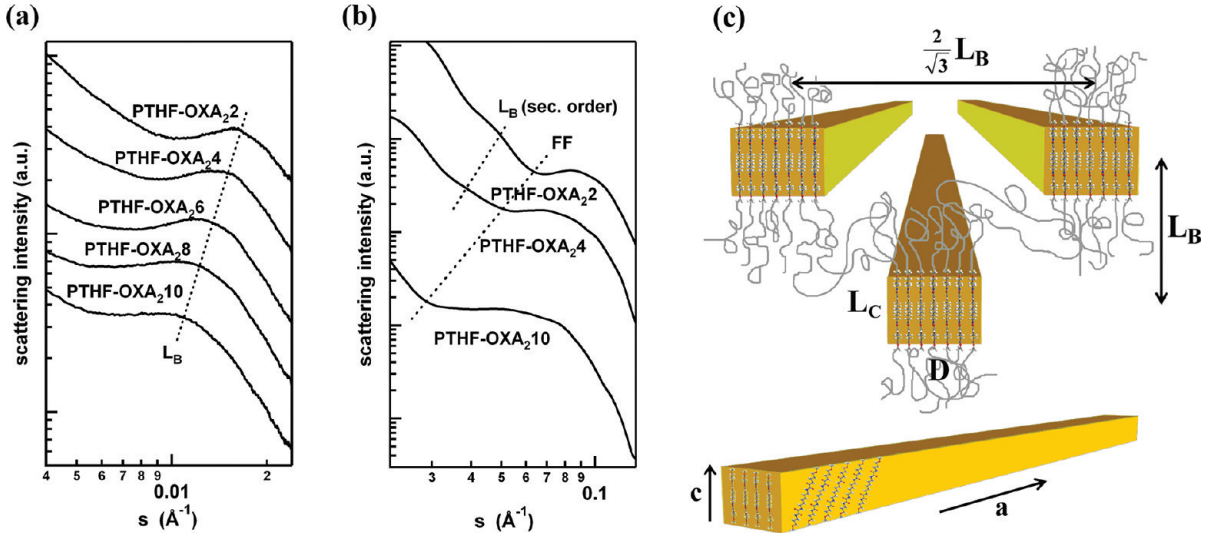

Figure 10. (a) SAXS intensities corresponding to bisoxalamide-based segmented poly(ether amide)s (**4a**−**e**). (b) Medium-angle scattering intensities for bisoxalamide based segmented poly(ether amide)s (**4a**,**b**,**e**) extracted from WAXD curves. (c) The model of hexagonally packed fibrillar crystals used to interpret the SAXS data.

WAXD. A 2D diffractogram of the uniaxially oriented compound **8** is presented in Figure 7. The fiber pattern was indexed to an orthorhombic unit cell with a = 5.05 Å, b = 10.00 Å, and c = 21.98 Å. With two monomers per unit cell the calculated density of the crystal amounts to 1.06 g cm^{-3}. The reflection indices and their calculated and experimental spacings are collected in Figure 7.

The 2D WAXD pattern exhibits a series of strong equatorial peaks that can be assigned to a smectic-like structure, the period of which is close to the long molecular dimension (***c***-direction). The two other directions likely correspond to the molecular width within the hydrogen-bonded planes (***a***-direction) and an integer number of the hydrogen-bonded sheet thickness (***b***-direction). Such stacking pattern is also preambled by scanning tunneling microscopy experiments on bis-urea model compounds by van Esch et al.[54]

The ***a*** parameter corresponding to interchain distance is ca. 5 Å, which is in agreement with values reported in literature.[38] The value of the ***b*** parameter corresponds to twice the thickness of a hydrogen-bonded sheet. The sheet thickness is higher than found for example in Nylon-6,2 (4.04 Å).[55] This increase probably reflects a slight nonplanarity of the molecular conformation. However, the exact deviation of the molecular conformation from the all-trans conformation is difficult to quantify at this stage.

A sketch of the crystalline structure of compound **8** is depicted in Figure 8. The length of the fully extended molecule is 28.75 Å, whereas the c parameter of the lattice equals 21.89 Å. In additional experiments (data not shown here) the X-ray diffraction of an oriented copolymer PTHF-OXA$_2$6 (**4c**) revealed a molecular tilt of the bisoxalamide blocks of 25° with respect to the normal to smectic layers. Therefore, the 3-methoxypropyl tails have to be inclined at a bigger angle in order to match the experimental c parameter (Figure 8). However, the exact conformation of the end groups with respect to the central bisoxalamide block has not been determined.

dx.doi.org/10.1021/ma2022309 | *Macromolecules* 2012, 45, 3948−3961

The WAXD curves of the model compound and the corresponding segmented poly(ether amide) **4c** are depicted in Figure 9a. The diffraction peaks of the bisoxalamide model compound are almost absent in the scattering plot of the corresponding copolymer and only a broad amorphous halo originating from the PTHF phase is visible. This can be explained by the small crystal size along the ***c***-direction. The maximum on top of the amorphous halo at 4.36 Å corresponds to the 110 peak, whereas the small maximum at 2.57 Å is the 200 peak. Since the reciprocal space vectors corresponding to these diffraction peaks are oriented perpendicular to the ***c***-direction, the crystal size along these directions can be much larger. WAXD profiles corresponding to segmented poly(ether amide)s **4a**−**4e** are given in Figure 9b. The curves of **4c**−**4e** exhibit the characteristic peak at 4.36 Å, while for **4a** and **4b** this peak is absent from the diffractograms. This fact can be explained, on the one hand, by the relatively higher weight contents of the hard block in these compounds (Table 1) and, on the other hand, by a possible difference in the corresponding unit cells of the hard block crystals.

It can be suggested that the long direction of the fibrillar crystals is in the *a*-direction, i.e., the direction of the hydrogen-bonded sheets, which is parallel to the extruded fiber axis. This conclusion is in agreement with the results obtained for an oriented fiber of model compound MeOProp-OXA$_2$6-ProOMe using polarized Raman spectroscopy (see the Supporting Information).

SAXS. Room-temperature SAXS curves are presented in Figure 10a. The scattering intensity is plotted as a function of the norm of the scattering vector ***s***. The SAXS curves show one interference maximum indicative of stacking of the phase-separated domains. Based on the fibrillar structure observed by AFM, the SAXS curves can be interpreted in terms of a 2D model (and not the conventional 1D model describing the lamellar structures) as schematically illustrated in Figure 10c.

Here it is assumed that the crystalline domains are much longer in one direction than in the two others and can therefore be considered as virtually infinite fibrils. The microstructural parameters of the samples (Figure 10c) such as the long spacing (L_B), crystal thickness (L_c), and amorphous domain thickness (L_a) can be derived from the SAXS curves in the approximation of a hexagonal packing of the fibrillar crystals. The L_B corresponds to the position of the Bragg peak (Figure 10a), whereas the crystalline domain thickness (L_c) was calculated from the position of the form factor (FF) visible in the medium-angle range (Figure 10b). The scattering intensity in the neighborhood of the form factor minimum was approximated with the expression

$$I(s) \propto \frac{1}{s^2}\left(\frac{\sin(\pi s L_c)}{\pi s L_c}\right)^2 \tag{1}$$

The crystal width D was calculated from the crystalline volume fraction Φ_{vol} of the bisoxalamide vs PTHF and the of L_B and L_c values as follows:

$$\Phi_{vol} = \frac{S_{crystalline\ core}}{S_{lattice\ surface}} \tag{2a}$$

$$\frac{\frac{M_{bisoxalamide}}{\rho_{bisoxalamide}}}{\frac{M_{bisoxalamide}}{\rho_{bisoxalamide}} + \frac{M_{PTHF}}{\rho_{PTHF}}} = \frac{L_c D}{\frac{2}{\sqrt{3}} L_B^{\,2}} \tag{2b}$$

$$D = \frac{\Phi_{vol}\frac{2}{\sqrt{3}} L_B^{\,2}}{L_c} \tag{2c}$$

Here ρ is the density (0.982 and 1.21 g cm^{-3} for amorphous PTHF and bisoxalamide segments, respectively), $S_{crystalline\ core}$ is the surface per crystal core, and $S_{lattice\ surface}$ is the total surface of the 2D lattice formed by the fibrils assuming hexagonal packing of the crystals.

The long spacing L_B, the lateral crystal dimensions (L_c and D), and the amorphous thickness (L_a) of the segmented poly(ether amide)s are given in Table 3. As expected, L_c and L_B increase with the number of methylene groups in the hard segment. The L_c is in good agreement with the theoretically calculated hard block length assuming a fully extended planar zigzag conformation. Moreover, the crystal width D ranging between 60 and 87 Å corresponds to a stack of 10−20 hydrogen-bonded sheets. The amorphous layer thickness L_a also increases with increasing spacer length, which is somehow unexpected since the soft segment length in all polymers is identical and equal to M_n = 1.1 × 10^3 g mol^{-1}. A possible explanation can be that the segment tilt influences the local density of the PTHF at the crystal−amorphous interface, which results in a change of the total amorphous layer thickness.

Table 3. Long Spacing (L), Crystalline Lamellar Thickness (L_c and D), and Amorphous Lamellar Thickness (L_a) for the Bisoxalamide-Based Segmented Poly(ether amide)s (4a−e)

	L_B (Å)	L_c (Å)	D (Å)	L_a (Å)	tilt angle[a] (deg)	hard block length[b] (Å)
4a	65.1	15.2[c]		50	16	12.5
4b	69.6	15.3	54	54.3	21	15
4c	75.7	16.5	64	59.2	25	17.5
4d	86.9	19.2	79	67.7	30	20
4e	95.3	22.6	87	72.7	32	22.5

[a]The chain tilt determined from the SAXS patterns of oriented copolymers (not shown here). [b]The hard block is defined here as the part of the molecule delimited by the hydrogen bonds; it is assumed that it is in the extended-chain conformation. [c]The distance determined from the SAXS patterns of oriented copolymer.

In order to correlate the thermal behavior of the segmented poly(ether amide) hard segments, observed with variable temperature FT-IR and DSC, with the evolution of the fibrillar crystalline structure, temperature-resolved SAXS measurements were performed. In Figure 11a, the scattering intensity is given as a function of temperature for polymer **4c**. It is clearly visible that during heating the interference maximum indicative of the phase-separated morphology disappears at 165 °C, marking the melting point of the bisoxalamide segments. In Figure 11b, the reverse of the first derivative of the SAXS invariant (Q) is given as a function of temperature for samples **4a**−**e**. The maximum of the curves observed in the range from 163 up to 220 °C corresponds to a rapid decrease of Q. The peak temperatures are in agreement with the temperature having the maximum decreasing rate of the hard segment crystallinity as measured by FT-IR and melting endotherm as measured by DSC (Figure 11b). Although FT-IR revealed the presence of hydrogen bonds well above the melting temperature (Figure 5), no structural features are observed in SAXS, suggesting the homogeneous state of the melt (Figure 11a).

Dynamic Mechanical Properties. The effect of temperature on polymer properties was studied by dynamic

dx.doi.org/10.1021/ma2022309 | Macromolecules 2012, 45, 3948−3961

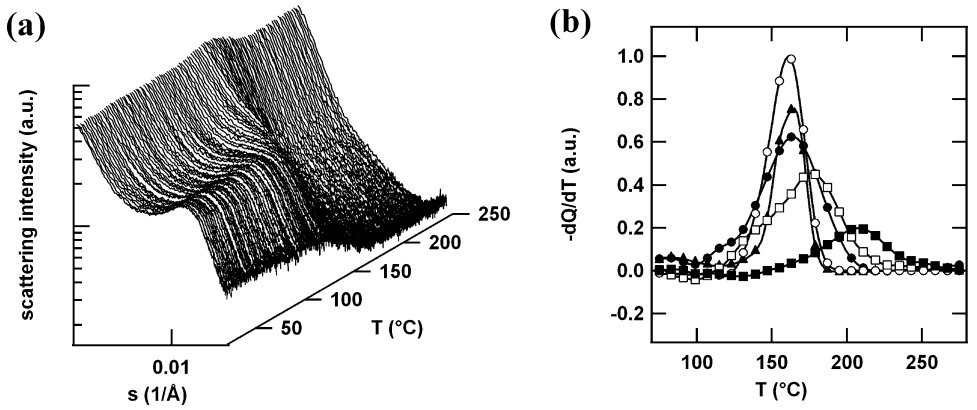

Figure 11. (a) Scattering intensity plots as a function of temperature for PTHF-OXA$_2$6 (**2c**). (b) The negative of the first derivative of the scattering invariant dQ/dT as a function of temperature for segmented poly(ether amide)s: (■) PTHF-OXA$_2$2 (**4a**), (□) PTHF-OXA$_2$4 (**4b**), (●) PTHF-OXA$_2$6 (**4c**), (○) PTHF-OXA$_2$8 (**4d**), and (▲) PTHF-OXA$_2$10 (**4e**).

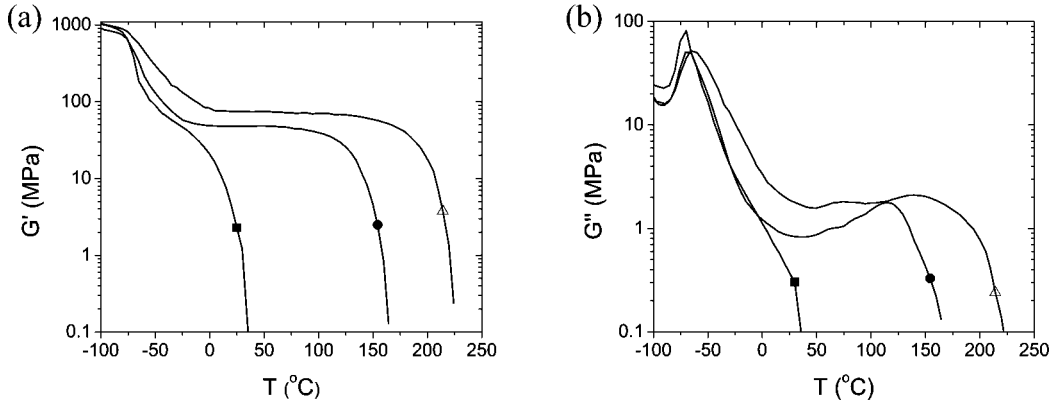

Figure 12. Storage modulus (G') and loss modulus (G'') as a function of temperature: (■) PTHF-OXA (**2**), (●) PTHF-OXA$_2$6 (**4c**), and (△) PTHF-OXA$_3$66 (**6**).

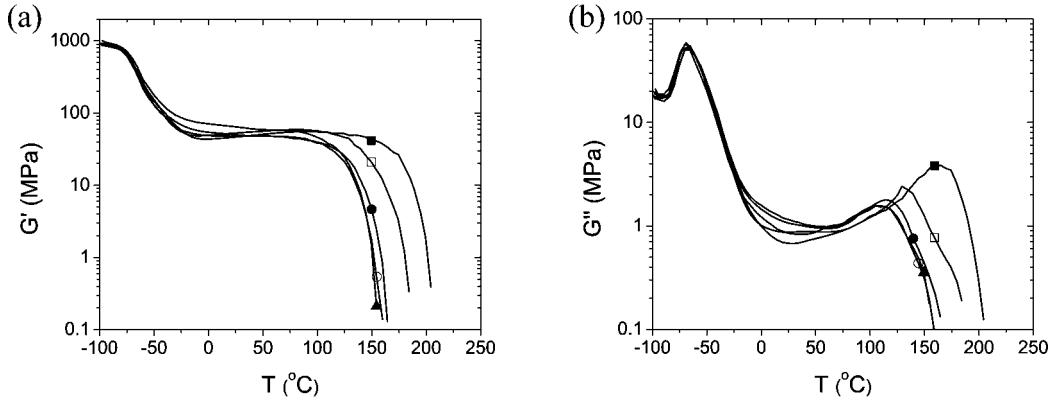

Figure 13. Storage modulus (G') and loss modulus (G'') as a function of temperature: (■) PTHF-OXA$_2$2 (**4a**), (□) PTHF-OXA$_2$4 (**4b**), (●) PTHF-OXA$_2$6 (**4c**), (○) PTHF-OXA$_2$8 (**4d**), and (▲) PTHF-OXA$_2$10 (**4e**).

mechanical analysis (DMA). The storage modulus and loss modulus of the segmented poly(ether amide)s (**2**, **4a**−**e**, and **6**) as a function of the temperature are depicted in Figures 12 and 13, respectively.

The glass transition temperature (T_g) of all segmented poly(ether amide)s are in between −70 and −65 °C. Interestingly, the T_g of PTHF is −86 °C,[56] which indicates that the segmented copolymers are highly phase separated. The rubber plateau starts at temperatures below 0 °C. Except for the segmented poly(ether amide) comprising single oxalamide groups (**2**), all polymers show a broad and fairly constant rubber plateau which is typical for segmented block copolymers with uniform hard segments. The storage modulus at 25 °C, which is a measure of the stiffness, increases with increasing number of oxalamide groups in the hard segment and can be ascribed to an increasing hard segment content. No correlation was found between spacer length and the rubber modulus which ranges from 48 to 65 MPa for polymers **4a**−**e**.

The rubber plateau is followed by a drastic drop in modulus, indicating softening of the polymer and thus melting of the

dx.doi.org/10.1021/ma2022309 | *Macromolecules* 2012, 45, 3948−3961

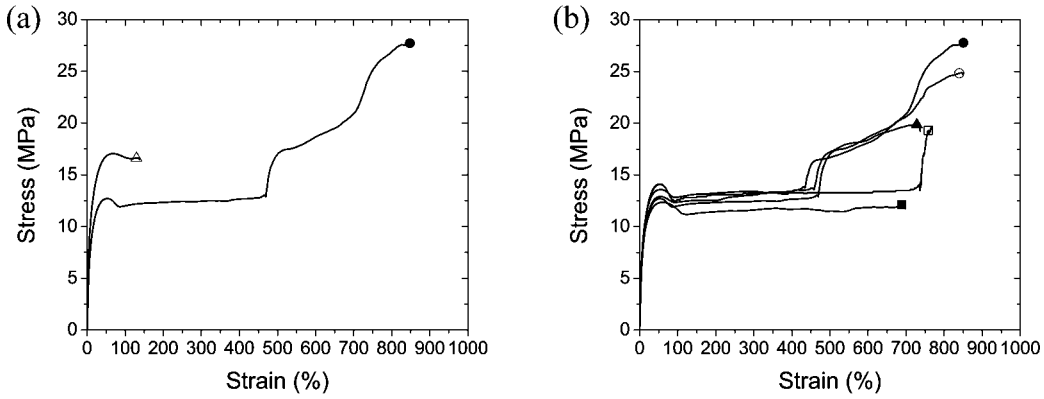

Figure 14. Stress–strain curves of the segmented poly(ether amide)s: (a) (●) PTHF-OXA$_2$6 (**4c**), (△) PTHF-OXA$_3$66 (**6**), (b) (■) PTHF-OXA$_2$2 (**2a**), (□) PTHF-OXA$_2$4 (**4b**), (●) PTHF-OXA$_2$6 (**4c**), (○) PTHF-OXA$_2$8 (**4d**), and (▲) PTHF-OXA$_2$10 (**4e**).

Table 4. Dynamic Mechanical and Mechanical Properties of Segmented Poly(ether amide)s 2, 4a–e, and 6

	hard segment										
	content(wt %)	w_c[a] (%)	T_g (°C)	$G'_{25\ °C}$ (MPa)	T_{flow} (°C)	E (MPa)	E/G'	σ_{yield} (MPa)	ε_{yield} (%)	$\sigma_{fracture}$ (MPa)	$\varepsilon_{fracture}$ (%)
2	7.3		−70	2	25						
4c	18.9	66	−70	48	160	135 ± 7	2.8	12.7 ± 0.1	56 ± 2	27.1 ± 0.6	800 ± 45
6	28	75	−65	75	220	235 ± 15	3.1	16.9 ± 0.1	64 ± 6	16.2 ± 0.4	107 ± 16
4a	15.4	90	−70	46	200	146 ± 20	3.2	12.3 ± 0.2	57 ± 3	11.4 ± 0.4	400 ± 180
4b	17.2	85	−70	53	180	147 ± 21	2.8	12.8 ± 0.2	55 ± 3	16.9 ± 3.9	700 ± 85
4c	18.9	66	−70	48	160	135 ± 7	2.8	12.7 ± 0.1	56 ± 2	27.1 ± 0.6	800 ± 45
4d	20.5	67	−65	49	150	121 ± 18	2.5	13.0 ± 0.2	56 ± 2	23.3 ± 1.7	770 ± 59
4e	22.1	85	−65	65	150	168 ± 9	2.6	13.5 ± 0.2	53 ± 3	18.5 ± 0.9	650 ± 78

[a]Hard segment ordering as determined in FT-IR spectra.

hard segments. The flow temperatures of the copolymers **4a–e** increase from 150 to 200 °C as the number of methylene groups between two oxalamide groups decreases. The segmented poly(ether amide) with three oxalamide groups in the hard segment (**6**) flows at a temperature of 220 °C.

Mechanical Properties. The tensile properties were studied using compression-molded bars cut to dumbbells (ISO37 s2). No tensile experiments were performed on the poly(ether amide) **2** as the stickiness of the material hindered sample preparation. Typical stress–strain curves are presented in Figure 14.

The *E*-modulus was determined at small deformations where stress linearly increases with strain. The *E*-modulus (E) and rubber modulus (G') are related according to

$$E = 2G'(1 + \nu) \quad (3)$$

with ν as the Poisson ratio.[57]

For incompressible materials, like elastomers, no volume change on deformation occurs and the Poisson ratio is 0.5. The relation between E/G' for such polymers is ∼3. It should be noted that the *E*-modulus is determined at 0.1–0.25% strain and the rubber modulus is determined at 0.1% torsion. Not surprisingly, the values of the *E*-modulus follow the same trends as observed for the rubber modulus.

As the stress increases, the stress–strain curves deviate from Hookean behavior and the materials starts to deform permanently. In all cases, the segmented poly(ether amide)s show pronounced yield points at about 50% strain followed by necking and by an upturn in the force deflection curve at the end of the necking process before fracture of the test specimen occurs. This behavior may be associated with the presence of long-range hard segment connectivity and a well percolated hard phase throughout the soft matrix.[31,57–59] Just above the yield point, the well-percolated hard phase disrupts and the fiber-like nanocrystals break up in their lateral direction. At strains higher than 400%, the segmented poly(ether amide)s with spacer length x = 6, 8, and 10 (**4c–e**) showed strain hardening, while strain hardening was absent or started above 700% strain for the polymers with a spacer length of x = 2 and 4 (**4a**,**b**). The segmented poly(ether amide)s **4a–e** have strains at break between ∼700 and 900% and stresses at break ranging from 11.7 to 27.5 MPa, depending on the presence of a strain hardening effect. The stress and strain at break of the segmented poly(ether amide) comprising three oxalamide groups (**6**) is 16.6 MPa and 130%, respectively.

Rheology. The morphology of a segmented block copolymer changes above the melting temperature of the hard segments from a microphase-separated material to a homogeneous melt.[60] The temperature at which this phenomenon occurs is called the microphase separation transition (MST). A method to determine this transition is to measure the storage modulus (G') as a function of temperature. The MST can be identified by a sharp rise in the storage modulus upon cooling as is illustrated in Figure 15 for different bisoxalamide polymers. The MSTs correspond well with the onset of crystallization transition temperatures found with DSC (Table 5). In addition—although we did not perform simultaneous spectroscopic experiments on the same sample—the built of elastic modulus (G') from an homogeneous viscous melt is associated with the appearance of X-ray scattering of the polymer and the formation of H-bonded and well-organized bisamide segments in FT-IR. The physical properties of those novel bisoxalamide elastomers thus stem

dx.doi.org/10.1021/ma2022309 | *Macromolecules* 2012, 45, 3948–3961

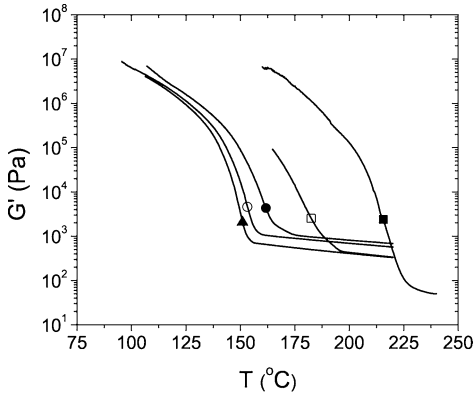

Figure 15. Temperature sweep with a frequency of 10 rad s^{-1} and a strain of 20% of bisoxalamide-based segmented poly(ether amide)s (■) PTHF-$OXA_2$2 (**4a**), (□) PTHF-$OXA_2$4 (**4b**), (●) PTHF-$OXA_2$6 (**4c**), (○) PTHF-$OXA_2$8 (**4d**), and (▲) PTHF-$OXA_2$10 (**4e**).

Table 5. Onset Temperatures (T_{onset}) and Microphase Separation Transition Temperature (T_{mst}) of Segmented Poly(ether amide)s 4a−e

	DSC T_{onset} (°C)	rheology T_{mst} (°C)
PTHF-$OXA_2$2 (**4a**)	216	∼225
PTHF-$OXA_2$4 (**4b**)	181	191
PTHF-$OXA_2$6 (**4c**)	162	170
PTHF-$OXA_2$8 (**4d**)	150	160
PTHF-$OXA_2$10 (**4e**)	147	155

from physical cross-linking by phase segregation into a bisoxalamide array, H-bond-driven superstructure.

CONCLUSIONS

Novel segmented poly(ether amide)s based on flexible PTHF segments and uniform rigid oxalamide hydrogen-bonding arrays were prepared. By changing the number of oxalamide groups in the hard segment and by changing the spacer length between two oxalamide groups for one sample series, the hard segment composition was varied. The polymer built with single oxalamide units between PTHF blocks is a sticky transparent solid material with a melting temperature around room temperature. Segmented poly(ether amide)s consisting of polytetrahydrofuran soft segments and uniform hard segments comprising at least two oxalamide groups are highly phase-separated TPEs with a broad temperature-independent rubber plateau. The melting temperatures of the bisoxalamide-based PEAs increase from 140 to 200 °C when the number of methylene groups between the two bisoxalamide groups decreased from 10 to 2. The copolymer with three oxalamide groups in the hard segment has a melting temperature of 220 °C. FT-IR revealed that the bisoxalamide-based hard segments are strongly hydrogen bonded and highly ordered. The bisoxalamide segments form fiber-like nanocrystals which are dispersed in the polytetrahydrofuran matrix. The long dimension of the crystals is parallel to the direction of the hydrogen bonds. One of the two small dimensions of the crystal approximately equals the length of one bisoxalamide segment, whereas the other one corresponds to the height of stacks of hydrogen-bonded sheet containing ca. 10−20 sheets. The hydrogen-bonding distance and intersheet distance are both ∼5 Å. The segmented copolymers have temperature-independent rubber plateaus starting at low temperatures. Temperature-dependent FT-IR, SAXS, and melt rheology data revealed broad hard segment melting transitions with formation of homogeneous melts. Segmented copolymers with two and three oxalamide groups in the hard segments have an elastic modulus between 121 and 210 MPa, a stress at break ranging from 15 to 27 MPa, and strain at break of 150 up to 900%. In all cases the polymers showed a distinct yield point indicative of long-range hard segment connectivity and a well-percolated hard phase throughout the soft polymer matrix. It can be concluded that hard segments comprising two or three oxalamide groups provide segmented poly(ether amide)s with good thermal and mechanical properties.

ASSOCIATED CONTENT

Supporting Information

Synthesis and characterization of polymers **2**, **4a−e**, and **6** and model compound **8** and polarized Raman spectra. This material is available free of charge via the Internet at http://pubs.acs.org.

AUTHOR INFORMATION

Corresponding Author

*Tel +31-53-4893004, Fax +31-53-4892155, e-mail p.j.dijkstra@utwente.nl.

Notes

The authors declare no competing financial interest.

ACKNOWLEDGMENTS

We thank Hetty ten Hoopen for the AFM measurements and Marlies Totte-van't Westeinde for the rheology measurements. This research was financially supported by the DOW Chemical Company under research agreement 218193. M.R., Y.O., and D.A.I. acknowledge the French Agence Nationale de la Recherche (SPIRWIND project of the HABISOL program and T2T project of the Blanc International program) for financial support. The authors are also grateful to Wim Bras and Giuseppe Portale from the DUBBLE beamline (ESRF, France) for fruitful discussions and excellent technical support.

REFERENCES

(1) Fakirov, S. *Handbook of Condensation Thermoplastic Elastomers*; Wiley-VCH: Weinheim, 2005.
(2) Holden, G.; Legge, N. R.; Quirk, R. P.; Schroeder, H. E. *Thermoplastic Elastomers*, 2nd ed.; Hanser Publishers: Munich, 1996.
(3) Cella, R. J. *J. Polym. Sci., Symp.* **1973**, *42*, 727−740.
(4) Alberola, N. *J. Appl. Polym. Sci.* **1988**, *36*, 787−804.
(5) Bornschlegl, E.; Goldbach, G.; Meyer, K. *Prog. Colloid Polym. Sci., Suppl.* **1985**, *71*, 119−124.
(6) Di Lorenzo, M. L.; Pyda, M.; Wunderlich, B. *J. Polym. Sci., Part B: Polym. Phys.* **2001**, *39*, 1594−1604.
(7) Di Lorenzo, M. L.; Pyda, M.; Wunderlich, B. *J. Polym. Sci., Part B: Polym. Phys.* **2001**, *39*, 2969−2981.
(8) Faruque, H. S.; Lacabanne, C. *Polymer* **1986**, *27*, 527−531.
(9) Ghosh, S.; Khastgir, D.; Bhowmick, A. K. *Polymer* **1998**, *39*, 3967−3975.
(10) Godovsky, Y. K.; Yanul, N. A.; Bessonova, N. P. *Colloid Polym. Sci.* **1991**, *269*, 901−915.
(11) Hatfield, G. R.; Bush, R. W.; Killinger, W. E.; Roubicek, P. M. *Polymer* **1994**, *35*, 3943−3947.
(12) Hatfield, G. R.; Guo, Y. H.; Killinger, W. E.; Andrejak, R. A.; Roubicek, P. M. *Macromolecules* **1993**, *26*, 6350−6353.
(13) Hucher, C.; Eustache, R. P.; Beaume, F.; Tekely, P. *Macromolecules* **2005**, *38*, 9200−9209.
(14) McLean, R. S.; Sauer, B. B. *Macromolecules* **1997**, *30*, 8314−8317.

(15) McLean, R. S.; Sauer, B. B. *J. Polym. Sci., Part B: Polym. Phys.* **1999**, *37*, 859−866.
(16) Sakurai, K.; Amador, G.; Takahashi, T. *Polymer* **1998**, *39*, 4089−4094.
(17) Sauer, B. B.; McLean, R. S.; Thomas, R. R. *Polym. Int.* **2000**, *49*, 449−452.
(18) Sheth, J. P.; Xu, J. N.; Wilkes, G. L. *Polymer* **2003**, *44*, 743−756.
(19) Yang, I. K.; Tsai, P. H. *J. Polym. Sci., Part B: Polym. Phys.* **2005**, *43*, 2557−2567.
(20) Yu, Y. C.; Jo, W. H. *J. Appl. Polym. Sci.* **1995**, *56*, 895−904.
(21) Yu, Y. C.; Jo, W. H.; Lee, M. S. *J. Appl. Polym. Sci.* **1997**, *64*, 2155−2163.
(22) Harrell, L. L. *Macromolecules* **1969**, *2*, 607−612.
(23) Miller, J. A.; Lin, S. B.; Hwang, K. K. S.; Wu, K. S.; Gibson, P. E.; Cooper, S. L. *Macromolecules* **1985**, *18*, 32−44.
(24) Ng, H. N.; Allegrez, A. E.; Seymour, R. W.; Cooper, S. L. *Polymer* **1973**, *14*, 255−261.
(25) Niesten, M. C. E. J.; Feijen, J.; Gaymans, R. J. *Polymer* **2000**, *41*, 8487−8500.
(26) Niesten, M. C. E. J.; Gaymans, R. J. *J. Appl. Polym. Sci.* **2001**, *81*, 1372−1381.
(27) van der Schuur, M.; de Boer, J.; Gaymans, R. J. *Polymer* **2005**, *46*, 9243−9256.
(28) Versteegen, R. M.; Kleppinger, R.; Sijbesma, R. P.; Meijer, E. W. *Macromolecules* **2006**, *39*, 772−783.
(29) Versteegen, R. M.; Sijbesma, R. P.; Meijer, E. W. *Macromolecules* **2005**, *38*, 3176−3184.
(30) Yilgor, I.; Shaaban, A. K.; Steckle, W. P.; Tyagi, D.; Wilkes, G. L.; McGrath, J. E. *Polymer* **1984**, *25*, 1800−1806.
(31) Yilgor, I.; Yilgor, E. *Polym. Rev.* **2007**, *47*, 487−510.
(32) Tyagi, D.; Yilgor, I.; McGrath, J. E.; Wilkes, G. L. *Polymer* **1984**, *25*, 1807−1816.
(33) Biemond, G. J. E.; Feijen, J.; Gaymans, R. J. *J. Appl. Polym. Sci.* **2007**, *105*, 951−963.
(34) Bouma, K.; Wester, G. A.; Gaymans, R. J. *J. Appl. Polym. Sci.* **2001**, *80*, 1173−1180.
(35) Gaymans, R. J.; Dehaan, J. L. *Polymer* **1993**, *34*, 4360−4364.
(36) Husken, D.; Krijgsman, J.; Gaymans, R. J. *Polymer* **2004**, *45*, 4837−4843.
(37) Krijgsman, J.; Husken, D.; Gaymans, R. J. *Polymer* **2003**, *44*, 7573−7588.
(38) Coe, S.; Kane, J. J.; Nguyen, T. L.; Toledo, L. M.; Wininger, E.; Fowler, F. W.; Lauher, J. W. *J. Am. Chem. Soc.* **1997**, *119*, 86−93.
(39) Lauher, J. W.; Fowler, F. W.; Goroff, N. S. *Acc. Chem. Res.* **2008**, *41*, 1215−1229.
(40) Nguyen, T. L.; Fowler, F. W.; Lauher, J. W. *J. Am. Chem. Soc.* **2001**, *123*, 11057−11064.
(41) Karle, I. L.; Ranganathan, D. *Int. J. Pept. Protein Res.* **1995**, *46*, 18−23.
(42) Karle, I. L.; Ranganathan, D. *Biopolymers* **1995**, *36*, 323−331.
(43) Karle, I. L.; Ranganathan, D.; Shah, K.; Vaish, N. K. *Int. J. Pept. Protein Res.* **1994**, *43*, 160−165.
(44) Frkanec, L.; Zinic, M. *Chem. Commun.* **2010**, *46*, 522−537.
(45) Asin, L.; Armelin, E.; Montane, J.; Rodriguez-Galan, A.; Puiggali, J. *J. Polym. Sci., Part A: Polym. Chem.* **2001**, *39*, 4283−4293.
(46) Black, W. D.; Preston, J. *Man-Made Fibers. Science and Technology*; Interscience: New York, 1968.
(47) Schulze, H. Thermoplastic adhesive polyoxamide from polyoxypropylene polyamine. US 4 119 615, 1978.
(48) Meier, R. J. *Vib. Spectrosc.* **2005**, *39*, 266−269.
(49) Kohan, M. I. *Nylon Plastic Handbook*; Hansers Publisher: Munich, 1995.
(50) Skrovanek, D. J.; Howe, S. E.; Painter, P. C.; Coleman, M. M. *Macromolecules* **1985**, *18*, 1676−1683.
(51) Skrovanek, D. J.; Painter, P. C.; Coleman, M. M. *Macromolecules* **1986**, *19*, 699−705.
(52) Armelin, E.; Aleman, C.; Puiggali, J. *J. Org. Chem.* **2001**, *66*, 8076−8085.
(53) Shalaby, S. W.; Pearce, E. M.; Frederic, R. J.; Turi, E. A. *J. Polym. Sci., Part B: Polym. Phys.* **1973**, *11*, 1−14.
(54) van Esch, J.; De Feyter, S.; Kellogg, R. M.; De Schrijver, F.; Feringa, B. L. *J. Am. Chem. Soc.* **1997**, *3*, 1238−1243.
(55) Chatani, Y.; Ueda, Y.; Tadokoro, H.; Deits, W.; Vogl, O. *Macromolecules* **1978**, *11*, 636−638.
(56) van Krevelen, D. W.; te Nijenhuis, K. *Properties of Polymers*, 4th ed.; Elsevier: Amsterdam, 2009.
(57) Cowie, J. M. G. *Polymer: Chemistry & Physics of Modern Materials*, 2nd ed.; Blackie Academic & Professional: London, 1991.
(58) Das, S.; Cox, D. F.; Wilkes, G. L.; Klinedinst, D. B.; Yilgor, I.; Yilgor, E.; Beyer, F. L. J. *Macromol. Sci. Phys.* **2007**, *46*, 853−875.
(59) Das, S.; Yilgor, I.; Yilgor, E.; Inci, B.; Tezgel, O.; Beyer, F. L.; Wilkes, G. L. *Polymer* **2007**, *48*, 290−301.
(60) Veenstra, H.; Hoogvliet, R. M.; Norder, B.; de Boer, A. P. *J. Polym. Sci., Part B: Polym. Phys.* **1998**, *36*, 1795−1804.